Anat. Histol. Embryol. **36,** 328–331 (2007)
ISSN 0340–2096
doi: 10.1111/j.1439-0264.2007.00776.x

Department of Anatomy, Faculty of Veterinary Medicine, University of Murcia, Murcia, Spain

Computed Tomography (CT) of the Lungs of the Dog Using a Helical CT Scanner, Intravenous Iodine Contrast Medium and Different CT Windows

L. Cardoso[1], F. Gil[2], G. Ramírez[2], M. A. Teixeira[1], A. Agut[3], M. A. Rivero[4]*, A. Arencibia[4] and J. M. Vázquez[2]

Addresses of authors: [1]Veterinary Hospital of Canoas, Lutheran University of Brazil (ULBRA), Canoas, Brazil; [2]Department of Anatomy, University of Murcia, Murcia, Spain; [3]Veterinary Clinical Hospital, University of Murcia, Murcia, Spain; [4]Department of Morphology, University of Las Palmas de Gran Canaria, Las Palmas, Spain; *Corresponding author: e-mail: mrivero@dmor.ulpgc.es

With 3 figures

Received October 2005; accepted for publication October 2006

Summary

The aim of this study was to determine the accuracy of helical computed tomography (CT) for visualizing pulmonary parenchyma and associated formations in normal dogs. CT scan was performed by using intravenous contrast medium and by applying different types of CT windows: soft tissue and lung windows, and high-resolution computed tomography of the lung. This technique allowed, especially with lung window types, a good view of the parenchyma, bronchial tree, vascular structures and pleural cavity. The selected images, with high anatomical quality and tissue contrast, may be a reference for future clinical studies of this organ. Thus, helical CT is a promising non-invasive method of diagnosing a wide variety of pulmonary diseases in dogs.

Introduction

Computed tomography (CT) is a modern diagnostic imaging technique, especially suitable for use in human medicine, to evaluate different pathological processes of the lung: neoplasms, metastases, interstitial infiltrates, etc. (Remy-Jardin et al., 2003; Bna et al., 2005; Lemburg et al., 2005). However, there are very few anatomical and clinical studies of this organ that have been carried out in veterinary medicine with helical scanners (Waters et al., 1998), by administering intravenous contrast medium and by applying specific CT windows for their correct evaluation. In most of the anatomo-clinical studies of the thoracic cavity of the dog, first-generation scanners have been used with smaller resolution (Burk, 1991; Feeney et al., 1991; Smallwood and George, 1993; Stickle and Hathcock, 1993; Assheuer and Sager, 1997; Ottesen and Moe, 1998; Rivero, 2002; Rivero et al., 2005). Moreover, appropriate window widths (WW) and window levels (WL) have not always been contemplated in the analysis of the anatomical structures that are imaged. In this study, we outline an evaluation of the lungs of the dog by means of the helical CT scanner, by administering oral and vascular contrast medium, and by considering different window widths and window levels.

Materials and Methods

Four mature dogs were selected for this study, mixed breed males and females, with age ranging from 4 to 6 years, median body weight 15 to 20 kg and average height being 40 cm. Two of the dogs (one male and one female) had a deep narrow chest thoracic conformation and the other two dogs had a barrel-shaped thorax. All the animals were healthy, without apparent pathologies that could influence our results. The study was approved by the Animal Care Committee of Lutheran University of Brazil. Immediately prior to scanning, the dogs were sedated with 0.2 mg/kg of acepromazine (Calmo Neosan; Pfizer, New York, NY, USA) and then anaesthetized with 15 mg/kg i.v. of pentobarbital sodium (Braun; Braun Medical, Tuttingen, Germany) and then intubated. An infusion of 800 mg/kg of iodine contrast medium (meglumine and sodium diatrizoate: Urografina, Schering, Madrid, Spain) was administered both per orally and intravenously through the cephalic vein to visualize the oesophagus and the thoracic vessels, respectively. Throughout the procedure, the animals were maintained in sternal recumbency position and, for a brief moment, they were hyperventilated and the CT images were obtained during the consequent apnoeic period.

Computed tomography was performed using a helical CT scanner (Toshiba Ex Vision; Toshiba Medical System, Tochigui, Japan) at the Radiology Institute 'Irion' of Porto Alegre, in Brazil. Transverse slices were acquired from the first thoracic vertebra to lumbo diaphragmatic recess with the following technical factors: a 1-s exposure time, 120 kV, 50 mA, 5 mm collimation/slice thickness, 2.5 mm slice distance, a pitch of 1, and high-spatial frequency reconstruction algorithm.

To appreciate the CT appearance of the lungs with different hypoattenuation shades, several CT windows were applied: soft tissue window (WW 652/WL-34), lung window (WW 928/WL-680), and a window with high-resolution computed tomography (HRCT) of the lung (WW 1085/WL-750). Of all the obtained CT images, four of each window type corresponding to different mediastinum levels were selected. Moreover, two enlarged details at the level of the caudal lobe of the right lung are included, one with the lung window and another with HRCT. The whole iconography of the work is always presented in cranial vision.

Results

In the CT images with the soft tissue window (Fig. 1), the parenchyma of the lungs appears hypoattenuated, making it difficult to specify the medial limits of the cranial lobes in the ventral part of the cranial mediastinum. The walls and the lumen of the thoracic portion of the trachea and of the main bronchi are not very well defined, for the similarity of

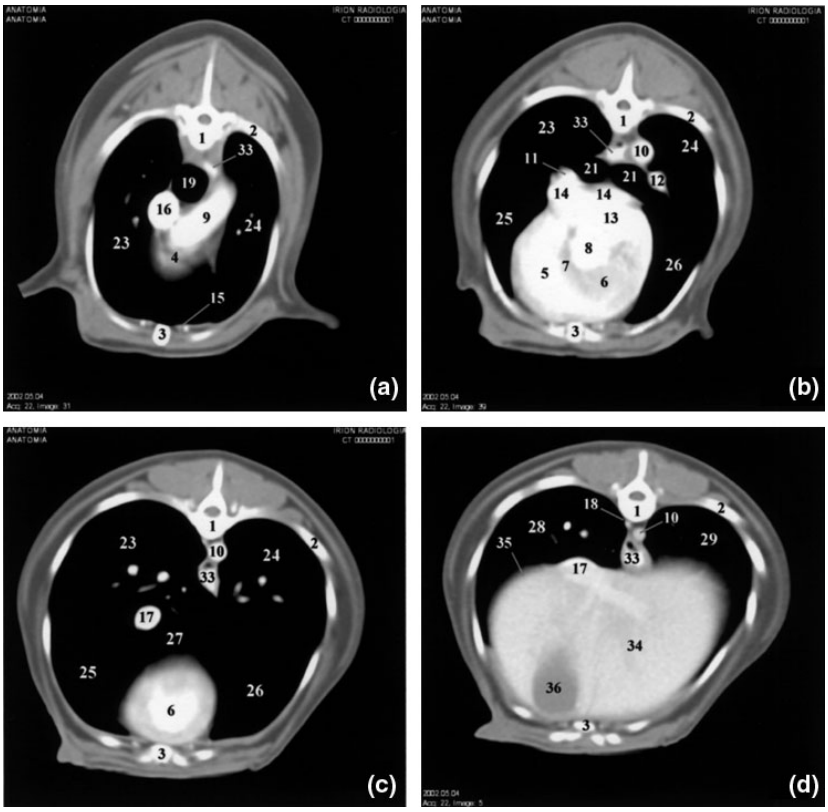

Fig. 1. Helical CT images of the thoracic cavity of the dog with soft-tissue window (WW-652/WL-34), after vascular injection with iodine contrast medium. Cranial vision; 1, thoracic vertebrae; 2, ribs; 3, sternum; 4, heart; 5, right ventricle; 6, left ventricle; 7, interventricular septum; 8, aortic bulb; 9, aortic arch; 10, thoracic aorta; 11, right pulmonary artery; 12, left pulmonary artery; 13, left atrium; 14, pulmonary veins; 15, internal thoracic artery and vein; 16, cranial cava vein; 17, caudal cava vein; 18, right azygous vein; 19, trachea: thoracic part; 20, tracheal carina; 21, principal bronchi; 22, lobar bronchi; 23, cranial lobe of the right lung; 24, cranial lobe of the left lung: cranial part; 25, right lung: middle lobe; 26, cranial lobe of the left lung: caudal part; 27, right lung: accessory lobe; 28, caudal lobe of the right lung; 29, caudal lobe of the left lung; 30; lobar arterial branches; 31, lobar pulmonary veins; 32, pleural cavity; 33, oesophagus: thoracic part; 34, liver; 35, diaphragm; 36; gall bladder.

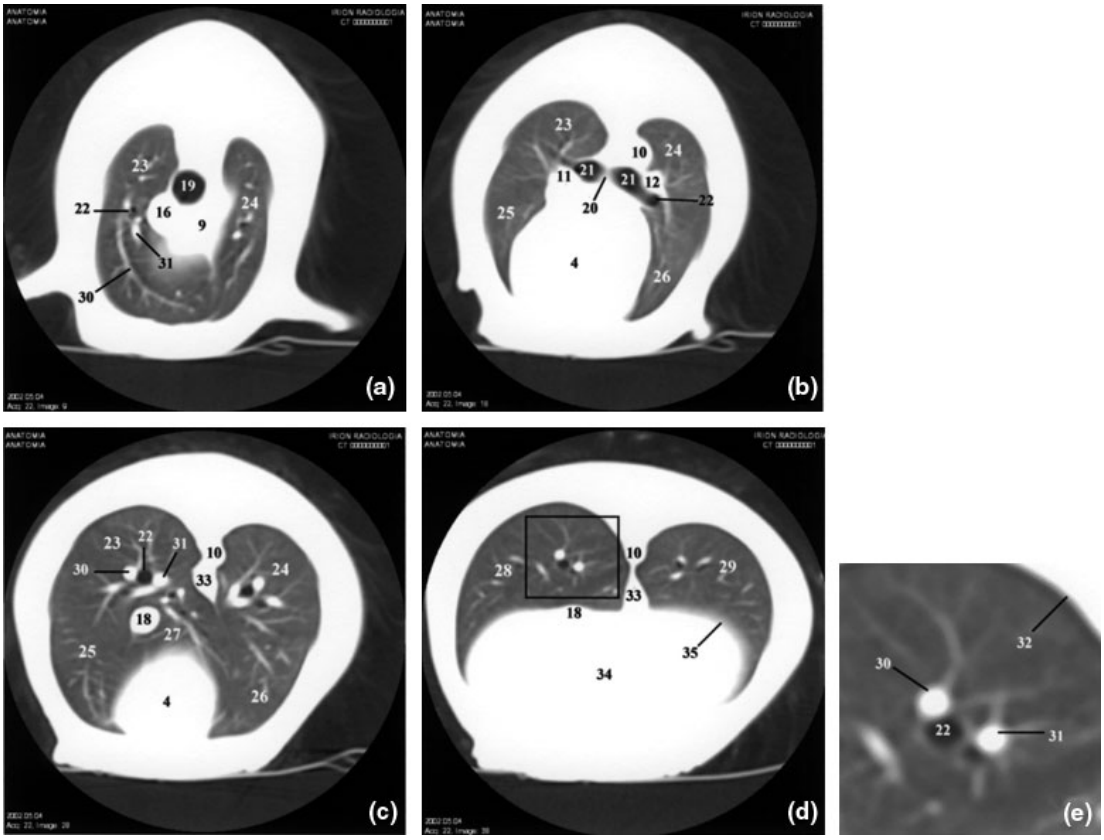

Fig. 2. Helical CT images of the thoracic cavity of the dog with lung window (WW-928/WL-680) after vascular injection with iodine contrast medium. The 2E CT image is an enlarged detail of the 2D CT image, at level of the square pointed out in the caudal lobe of the right lung. Cranial vision; for more details see Fig. 1.

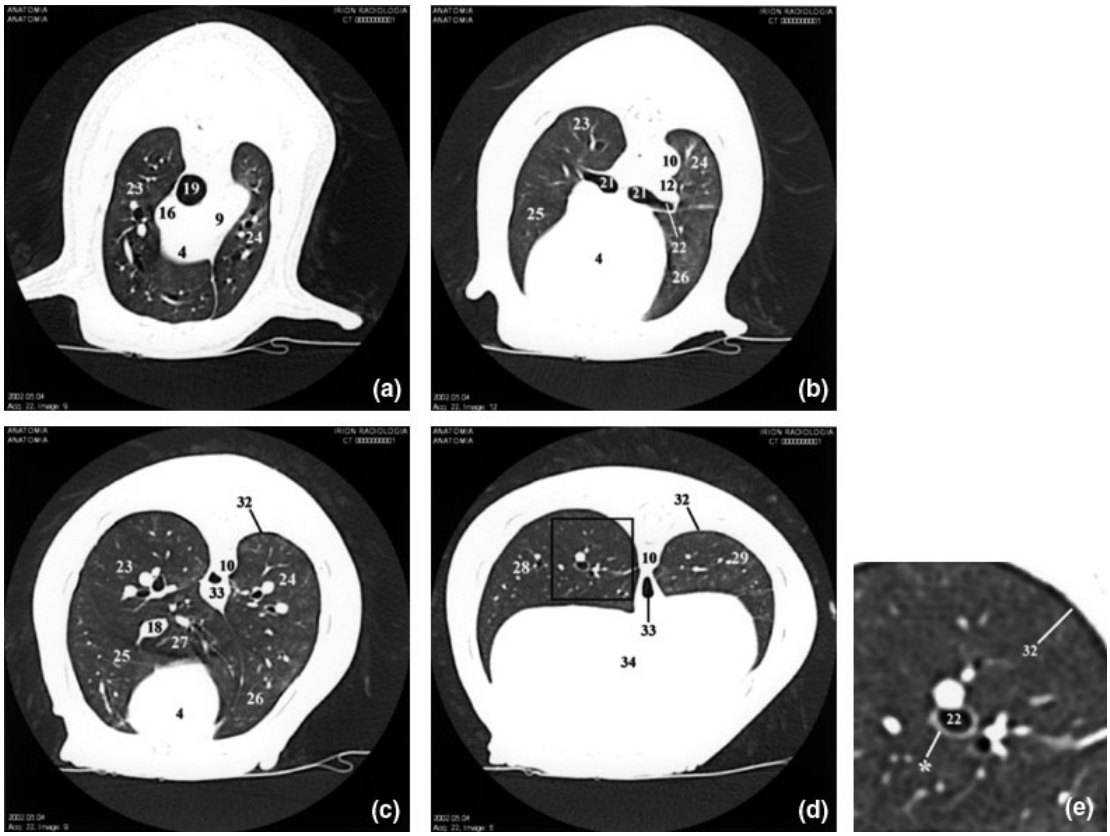

Fig. 3. Helical CT images of the thoracic cavity of the dog with high resolution CT (WW-1085/WL-750) after vascular injection with iodine contrast medium. The 3E CT image is an enlarged detail of the 3D CT image, at level of the square pointed out in the caudal lobe of the right lung, where it is appreciated with clarity the wall of the lobar bronchi. Cranial vision; for more details see Fig. 1.

hypoattenuation regarding the pulmonary parenchyma. Moreover, with this window type, the lobar bronchi cannot be visualized. The vascular formations of the lung are only clearly defined at the level of the hilus, because of deeper lumen and the use of intravenous contrast medium. Inside the parenchyma, the lobar pulmonary veins and the lobar branches of the pulmonary arteries are not very evident.

The degree of hypoattenuation of the lungs is not so intense with the lung window (Fig. 2). It allows a better definition of the cranial lobes and a better tomographical definition of the trachea, main bronchi and lobar bronchi, because all these structures present a higher radiotransparency than the lung. At the level of the pulmonary parenchyma, the vascular structures are better defined than in the rest of the applied CT windows. In this sense, it is possible to visualize the triad that comprises the lobar pulmonary vein, the lobar arterial branch and the lobar bronchus. The pleural cavity presents a light tomographic sign, not being observed in the soft tissue window.

In the HRCT images (Fig. 3), the shade of hypoattenuation or radiotransparency of the lungs is intermediate between the CT of soft tissue window and those of lung window; it allows a correct definition at the level of the pulmonary contours of the cranial lobes and of other lung lobes. With this technique and after the administration of intravenous contrast medium, the vascular formations are shown with greater CT density than in the CT images of lung window. Just as in the lung window, the tracheal lumen, as well as the lumen of the lobar and main bronchi, presents shades of very intense hypoattenuation, which facilitates its evaluation.

With the lung window images and the HRCT images, it is possible to recognize, at the level of the tracheal bifurcation, the tracheal carina, which is not observed with the soft-tissue window. On the other hand, with HRCT of the lung, we can have a more precise evaluation of the wall of the lobar bronchi, just as it is noticed in the 3E CT image (an enlarged detail of the 3D CT image), which is not very evident in the CT of lung window (2E CT image). Finally, as mentioned earlier, the pleural cavity is not visualized in the CT of soft-tissue window and presents certain definition in the lung window. On the contrary, in the HRCT set we can evaluate it like a hypoattenuated halo that contours the parenchyma.

Discussion

Computed tomography is said to be a revolutionary tool in the imaging of the pulmonary organ for clinical diagnosis (Johnson et al., 2004; Morandi et al., 2004; Zekas et al., 2005) and mediastinal pathologies (Essman et al., 2002; Yoon et al., 2004; Prather et al., 2005), because of its capacity to discriminate the different tissues. The CT technique by means of the CT window, also allows modification of the attenuation degree, inside some limits, to improve the definition of certain structures. This fact should be considered when the organs of the thorax are analysed, because of the wide range of CT numbers (HU) that present their tissues (Feeney et al., 1991; Ottesen and Moe, 1998).

On the other hand, the administration of an intravenous contrast medium contributes notably to the definition of the

main vascular formations and makes it possible to discern between normal and pathological vascular structures (Tarver and Conces, 1996). This contribution is more evident when helical scanners are used, even when administering a smaller quantity of contrast medium.

Of the literature surveyed, only Feeney et al. (1991) and Assheuer and Sager (1997) had applied the lung window in anatomical studies of the thoracic cavity. Stickle and Hathcock (1993) and Ottesen and Moe (1998) recommended it. This window allows the visualization of the functional distribution of the arteriovenous structures and of the bronchial tree, and also provides a certain definition of the pleural cavity (Haaga et al., 1996). The HRCT has not been considered in veterinary medicine, but it allows a more precise evaluation of the parenchyma of the lungs and, especially, the pleural cavity and the wall of the lobar bronchi. In this sense, we have used the slice thickness interval of 3–5 mm proposed for dogs by Stickle and Hathcock (1993) and Ottesen and Moe (1998), because we consider it appropriate for studying normal lungs. A smaller slice thickness (2–3 mm) is more suitable for evaluating lung diseases (Murata et al., 1988). In human medicine, HRCT with 1.5–3 mm collimation has become an integral tool for the evaluation of patients with diffuse lung diseases (Nakata et al., 1985). Recent CT scanner developments, which enable the use of < 1 mm collimation, have allowed a more precise evaluation of pulmonary parenchyma by reducing the partial volume effect and improving the spatial resolution (Nishimoto et al., 2005).

The improved quality and the absence of artefacts in our images are due to the type of the scanner used, the time of acquisition – 1 s, their obtainment in apnoeic phase, the correct anatomical symmetry during the positioning of the animals in sternal recumbency and the collimation or slice thickness.

Contrary to human medicine which routinely uses HRCT, veterinary medicine has not yet reached that high degree of development to be able to continuously use this technique, because of the high costs, handling problems and anaesthetic risks. Therefore, the CT images presented in this study try to serve as initial references for clinical CT imaging studies of the lungs of the dog and for interpreting lesions of the thoracic cavity and associated structures.

References

Assheuer, J., and M. Sager, 1997: Thorax. In: MRI and CT Atlas of the Dog, 1st edn (J. Asshener and M. Sager, eds). Berlin, Oxford: Blackwell Science Ltd., pp. 315–346.

Bna, C., M. Zompatori, F. Ormitti, N. Sverzellati, and A. Verduri, 2005: High resolution CT (HRCT) of the lung in adults. Defining the limits between normal and pathologic findings. Radiol. Med. (Torino) **109,** 460–471.

Burk, R. L., 1991: Computed tomography of thoracic diseases in dogs. J. Am. Vet. Med. Assoc. **199,** 617–621.

Essman, S. C., J. P. Hoover, R. J. Bahr, J. W. Ritchey, and C. Watson, 2002: An intrathoracic malignant peripheral nerve sheath tumor in a dog. Vet. Radiol. Ultrasound **43,** 255–259.

Feeney, D., T. Fletcher, and R. Hardy, 1991: Atlas of Correlative Imaging Anatomy of the Normal Dog: Ultrasound and Computed Tomography, 1st edn. Philadelphia, PA: WB Saunders Co.

Haaga, J. R., C. F. Lanzieri, D. J. Sartoris, and E. A. Zerhouni, 1996. Tomografía computerizada y resonancia magnética. Diagnóstico por imagen corporal total. Ed. Philadelphia, PA: Mosby.

Johnson, V. S., I. K. Ramsey, H. Thompson, T. A. Cave, F. J. Barr, H. Rudorf, A. Williams, and M. Sullivan, 2004: Thoracic high-resolution computed tomography in the diagnosis of metastatic carcinoma. J. Small Anim. Pract. **45,** 134–143.

Lemburg, S. P., T. Kagel, S. Grootonk, S. Ewig, T. T. Bauer, G. Schultze-Werninghaus, V. Nicolas, and C. M. Heyer, 2005: Non-passable tumor-associated stenosis of trachea and stent-implantation – an indication for virtual CT-bronchoscopy. Pneumologie **59,** 529–532.

Morandi, F., J. S. Mattoon, J. Lakritz, J. R. Turk, J. Q. Jaeger, and E. R. Wisner, 2004: Correlation of helical and incremental high-resolution thin-section computed tomographic and histomorphometric quantitative evaluation of an acute inflammatory response of lungs in dogs. Am. J. Vet. Res. **65,** 1114–1123.

Murata, K., A. Khan, K. A. Rojas, and P. G. Herman, 1988: Optimization of computed tomography technique to demonstrate the fine structure of the lung. Invest. Radiol. **23,** 170–175.

Nakata, H., T. Kimoto, T. Nakayama, M. Kido, N. Miyazaki, and S. Harada, 1985: Diffuse peripheral lung disease: evaluation by high-resolution computed tomography. Radiology **157,** 181–185.

Nishimoto, Y., M. Takahashi, K. Murata, and K. Kichikawa, 2005: Detectability of various sizes of honeycombing cysts in an inflated and fixed lung specimen: the effect of CT section thickness. Korean J. Radiol. **6,** 17–21.

Ottesen, N., and L. Moe, 1998: An introduction to computed tomography (CT) in the dog. Eur. J. Companion Anim. Pract. **8,** 29–36.

Prather, A. B., C. R. Berry, and D. E. Thrall, 2005: Use of radiography in combination with computed tomography for the assessment of noncardiac thoracic disease in the dog and cat. Vet. Radiol. Ultrasound **46,** 114–121.

Remy-Jardin, M., P. Dumont, and J. Remy, 2003: High-resolution computed tomography techniques in diffuse parenchymal lung disease and their application to clinical practice. Semin. Respir. Crit. Care Med. **24,** 333–346.

Rivero, M. A., 2002. Estudio morfológico del cuello, tórax y abdomen craneal en el perro (*C. familiaris*, L.), mediante tomografía computerizada. Doctorate Thesis, Spain: University of Las Palmas de Gran Canaria.

Rivero, M. A., J. A. Ramírez, J. M. Vázquez, F. Gil, G. Ramírez, and A. Arencibia, 2005: Normal anatomical imaging of the thorax in three dogs: computed tomography and macroscopic cross sections with vascular injection. Anat. Histol. Embryol. **34,** 215–219.

Smallwood, J. E., and T. F. George, 1993: Anatomic atlas for computed tomography in the mesaticephalic dog: thorax and cranial abdomen. Vet. Radiol. Ultrasound **34,** 65–83.

Stickle, R. L., and J. T. Hathcock, 1993: Interpretation of computed tomographic images. Vet. Clin. North Am. Small Anim. Pract. **23,** 417–435.

Waters, D. J., F. V. Coakley, M. D. Cohen, M. M. Davis, B. Karmazyn, R. Gonin, M. P. Hanna, D. W. Knapp, and S. A. Heifetz, 1998: The detection of pulmonary metastases by helical CT: a clinicopathologic study in dogs. J. Comput. Assist. Tomogr. **22,** 235–240.

Yoon, J., D. A. Feeney, D. E. Cronk, K. L. Anderson, and L. E. Ziegler, 2004: Computed tomographic evaluation of canine and feline mediastinal masses in 14 patients. Vet. Radiol. Ultrasound **45,** 542–546.

Zekas, L. J., J. T. Crawford, and R. T. O'Brien, 2005: Computed tomography-guided fine-needle aspirate and tissue-core biopsy of intrathoracic lesions in thirty dogs and cats. Vet. Radiol. Ultrasound **46,** 200–204.